

An abyssal topographic experiment*

W. JOHN GOULD†, ROSS HENDRY‡ and HERBERT E. HUPPERT§

(Received 3 April 1980; accepted 14 May 1980; in ed. 14 May to 4 December, 1981;
final revision received 29 January 1981)

Abstract—Observations have been made of the flow field and density structure surrounding a small isolated hill $20 \times 5 \text{ km} \times 500 \text{ m}$ on the Iberian Abyssal Plain in 5340-m depth. Typical flows far from the hill were from the west and south, and of the order of 2.5 cm s^{-1} at the level of the hill top. Near the hill the currents at this level were accelerated on the western flank and reduced to the east by an anticyclonic flow perturbation giving a velocity difference across the hill of 3 to 5 cm s^{-1} . CTD (conductivity-temperature-depth) profiles showed a doming of isotherms over the hill and potential temperatures on top of the hill that were as low as on the abyssal plain 500 m below. The profiles also revealed that topographically induced density perturbations penetrated to approximately 2.5 times the height of the hill above the abyssal plain. The observations compare reasonably with a theoretical stratified Taylor column model.

1. INTRODUCTION

THE DEPTH of the ocean bed varies significantly from place to place. This has been known for centuries. However, little is known about the many influences this variation in depth of the lower frictional boundary has on the overlying ocean. The ocean bottom is in general rough, with the roughness elements spanning a wide range of scales from small ripples to seamounts, ocean ridges, and continental slopes. The most frequent features in deep-ocean topography are abyssal hills (MENARD, 1964), which range horizontally up to a few tens of kilometres and in height to a few hundred metres. BELL (1975, 1979) statistically analysed profiles of deep-sea bathymetry in the North Pacific and found a k^{-2} power law dependence of squared amplitude with a flattening of the spectrum at wavenumbers below 0.025 cycles per kilometre (40 km wavelength). Other ocean basins may have bathymetric variations differing from the North Pacific, but North Atlantic observations suggest that the dimensions of the abyssal hills there are not greatly different (RONA, HARBISON and BUSH, 1974).

The interaction of oceanic flows with abyssal topography is important in a variety of subjects, including the interpretation of sediment distributions, the determination of rates

* Editor's note: The editor regrets his delay in editing this paper. It is the paper cited by W. B. OWENS and N. G. HOGG in their paper "Oceanic observations of stratified Taylor columns near a bump", *Deep-Sea Research*, 27, 1029-1045, 1980. The present paper was received by the editor on 3 April 1980 and the OWENS and HOGG paper was received on 16 July 1979. The complementary nature of the two papers is evident. The observations upon which the present paper is based were made in the spring and early summer of 1975, and a preliminary report of them was included in the MODE Hotline News, No. 77. The observations reported by OWENS and HOGG were made in October 1976 and July 1977.

† Institute of Oceanographic Sciences, Wormley, Godalming, Surrey GU8 5UB, U.K.

‡ Atlantic Oceanographic Laboratory, Bedford Institute of Oceanography, Dartmouth, Nova Scotia, Canada.

§ Department of Applied Mathematics and Theoretical Physics, University of Cambridge, Cambridge, U.K.

of vertical mixing of deep-ocean waters, and the parametrization of bottom boundary effects in deep-ocean circulation models. Almost all present day numerical models have vertical and horizontal grid sizes considerably larger than the size of typical topographic variations. The models include the effects of bottom roughness, if at all, in very simplified form (an *ad hoc* bottom friction is commonly used). However, recent theoretical analyses and observations indicate that bathymetric variations can have large influences on the flow field, not at all accounted for in the current numerical models. A better understanding of these influences is still needed and acts as part of the motivation for this work.

The interaction of steady flows with idealized topography has received attention from several authors. HOGG (1973a) and HUPPERT (1975) investigated the formation of a stratified Taylor column above isolated topography. HOGG (1973b) applied his analysis to explain the development of a deep well-mixed region in the northwest Mediterranean due to the Rhone fan and to the sediment distribution around a seamount (ROBERTS, HOGG, BISHOP and FLEWELLEN, 1974). Some effects of unsteady flows interacting with topography have been considered by HUPPERT and BRYAN (1976). They suggest that such interactions may cause deep-ocean eddies.

Actual observations of the interaction of mid-latitude oceanic flows with large-scale topography have been limited. MEINKE (1971) studied the flow around Meteor Seamount. VASTANO and WARREN (1976) examined the interaction of the Gulf Stream with the New England Seamount Chain. The flow and stratification around Bermuda were studied by HOGG, KATZ and SANFORD (1978) and circulation patterns in adjacent areas overlying both rough and smooth abyssal topography were compared during the Mid-Ocean Dynamics Experiment (MODE) by SWALLOW (1973).

Abyssal hills are so abundant on the deep-ocean floor that in many areas they form a continuous cover of the sea bed. Although of great importance for understanding ocean currents, it is these areas whose roughness must be parametrized in numerical methods, and critical studies are hindered by the interaction of one feature with another—each feature modifying the upstream flow that impinges upon its neighbour. A sensible first step thus seemed to be to study an isolated abyssal hill, one that might be considered typical of those in generalized rough topography but was far enough removed from its neighbours to be unaffected by them. Such a study could also be compared directly with theoretical calculations already carried out.

After investigation of possible sites near the British Isles, it was decided to conduct an experiment in the Iberian Abyssal Plain roughly from $41^{\circ}00'$ to $41^{\circ}40'N$ and from $13^{\circ}30'$ to $14^{\circ}30'W$.

The region chosen was close to that used in early trials of neutrally buoyant floats in 1958 (SWALLOW and HAMON, 1960). The 1958 soundings indicated the presence of isolated hills, separated by several "hill diameters" from their nearest neighbours, on an otherwise flat abyssal plain. The hills are of a fairly typical size. One hill centred on $41^{\circ}17'N$, $14^{\circ}00'W$ was chosen and nicknamed "Brontosaurus Bump". It is probably a basalt outcrop in the sedimentary plain. It is elongated with a length of 20 km along 020 to 200° , a width of 6 km, and rises 470 m above the plain. Southeast of it, a smaller hill, casually named "Webb's Foot", was discovered in echo soundings taken during the experiment. It measures 9×4 km \times 292 m. A contour map of "Brontosaurus Bump" and "Webb's Foot" is shown in Fig. 1 together with a general chart of the Iberian Abyssal Plain.

The observations were conducted in two legs during the spring of 1975: Cruise 70 of R.R.S. *Discovery* from 31 March to 21 April and Cruise 72 from 31 May to 25 June. Prior to

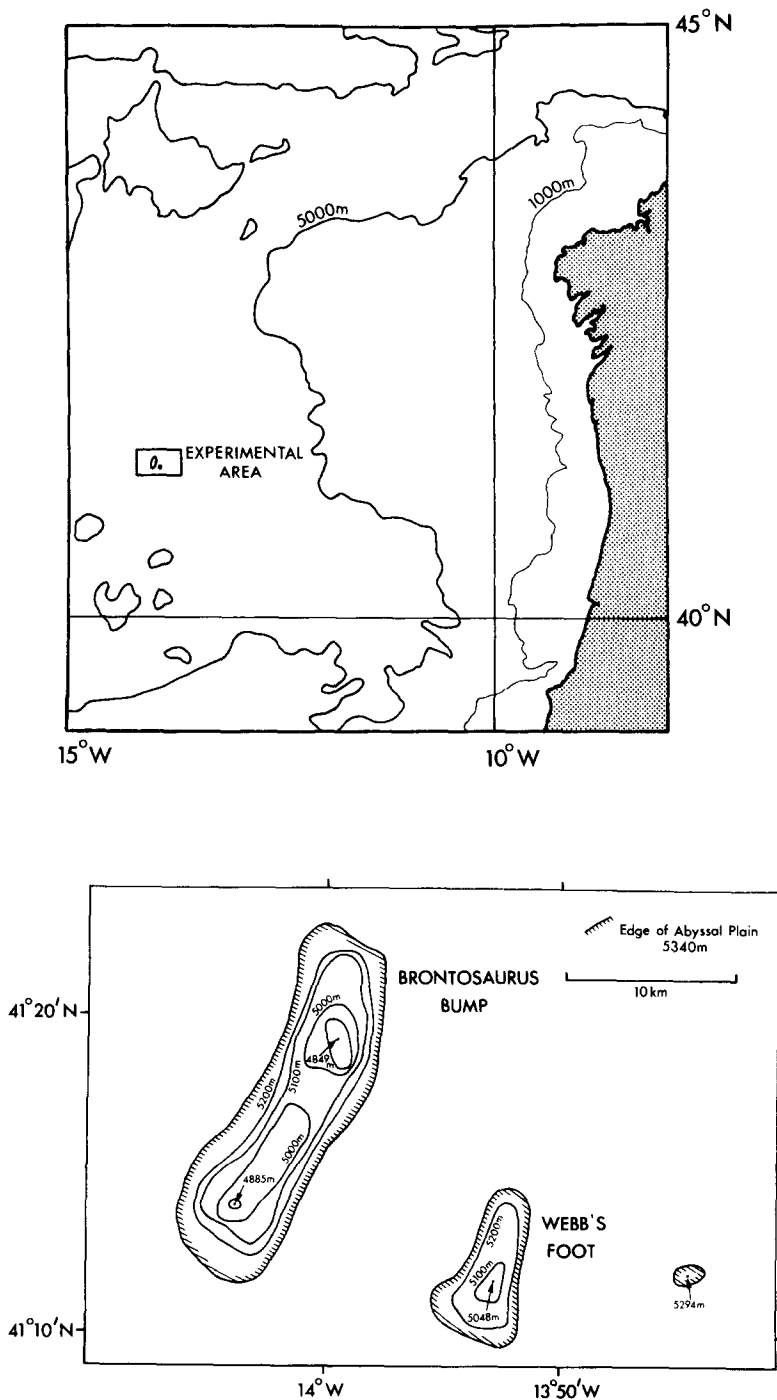


Fig. 1. Location of the experimental area in the northeast Atlantic Ocean and detailed bathymetry of the abyssal hills. The depth of the abyssal plain around the hill is 5340 m. The stippled region represents the Iberian Peninsula.

the start of Cruise 70 a near-bottom mooring with a single Aanderaa current meter was to be deployed for the duration of the observations and reveal the direction of the near-bottom currents. The data would then be used to decide upon the orientation of the main moored array.

Within the array of current meters, neutrally buoyant floats were to be tracked. These were of the type used in the MODE-1 experiment (SWALLOW, MCCARTNEY and MILLARD, 1974), but with the improvement of using acoustic navigation of the ship relative to three near-bottom moored transponders. The floats would serve to map the detailed flow around the hill in real time so that experimental tactics could be modified.

The structure of the density field from the surface to within a few tens of metres of the sea bed was measured using the WHOI/Brown CTD (BROWN and MORRISON, 1978) profiler with calibration samples taken by a rosette multisampler and reversing thermometers.

The preliminary mooring (187) was set on 13 March, 1975 rather than in mid-January as originally intended. When recovered on 31 March, the 5100-m depth record revealed predominantly northward flow with a mean speed close to 3.5 cm s^{-1} (but see the discussion below of possible errors in the direction measurements). As the purpose of the outer moorings was to determine the far-field flow, two of the three moorings were then placed upstream of "Brontosaurus Bump" and the third downstream. The inner moorings were set around the hill as indicated in Fig. 2.

The floats were set a few at a time, mostly at the 4800-m level to delineate the deep-flow pattern. CTD stations were made in conjunction with the float-tracking operations (SWALLOW *et al.*, 1974). (Early in Cruise 70 there were problems with the conductivity

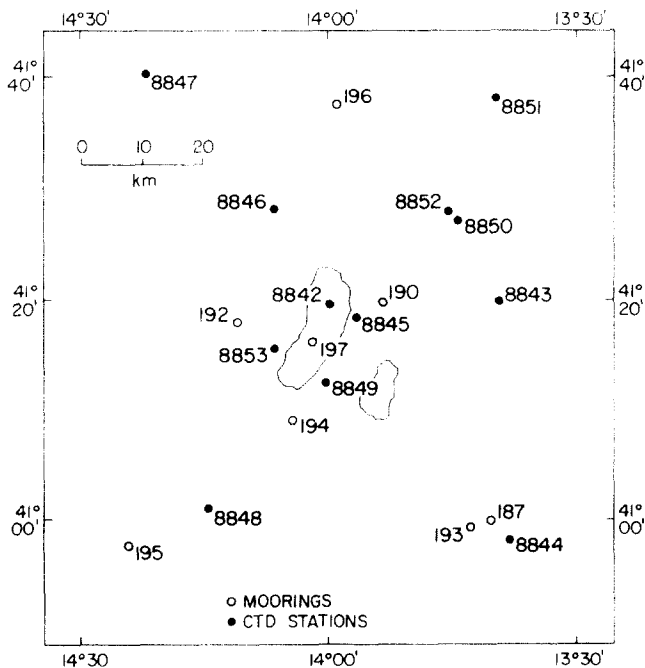


Fig. 2. Mooring and CTD station positions for R.R.S. *Discovery* Cruise 70. Outlines of the topography represent approximately the 5300-m contour above the 5340-m abyssal plain.

sensor of the CTD and eventually the sensor had to be removed. For the remainder of Cruise 70 only temperatures were measured.) All the floats were recovered prior to the end of the first cruise, but the current meter moorings were left in place.

On return to the area at the start of Cruise 72 (3 June) the moorings were in position and during the night of 3 to 4 June, a pattern of nine floats was set, ballasted for 4800 m. On interrogation of mooring 194 the release was inadvertently fired and the mooring recovered. It was set as mooring 199 later that day.

The tracking of floats and working of CTD stations continued uninterrupted until 11 June, apart from a brief break caused by a winch failure. On 11 June the ship had to leave the area to land two sick crewmen. On return to the area, some 50 h later, the floats were re-located and tracking continued.

All current meter moorings and all but one of the floats were recovered prior to the ship leaving the area on 22 June. The recovery of the floats was accomplished under difficult acoustic conditions. The one lost float was recovered from France early in 1977. A single mooring was left out at the end of the experiment but attempts to locate it in 1976 were unsuccessful.

This paper will consider only the data obtained during Cruise 70 (April 1975). The observations of Cruise 72 will be the subject of a second paper because during that cruise more temporal and spatial variation in the flow were observed and a separate discussion is needed. Sections 2, 3, 4, and 5 describe the theoretical background, the observations with neutrally buoyant floats, the moored current meter results, and the density (CTD) observations. The synthesis of the two types of velocity measurements, their relations to the density data, and the similarity to the theoretical background form the subject of section 6. The final section contains a summary of the experimental results and the conclusions drawn from them.

2. THE THEORETICAL BACKGROUND

The simplest interaction between mean currents and topography occurs when an effectively inviscid homogeneous current flows steadily towards a topographic feature, the breadth and width of which are comparable*. The resulting quasi-geostrophic response is independent of depth and is governed by the principle of conservation of potential vorticity. Because steadily oncoming vortex lines are squashed as they move over a (sufficiently small) topographic feature, conservation of mass requires that the horizontal extent of a column of specific fluid particles becomes larger and thus, by conservation of angular momentum, the fluid develops anticyclonic vorticity. The resulting flow field is a combination of the velocity induced by the anticyclonic vorticity and the oncoming velocity. This results in an enhanced flow to the left (looking downstream) of the feature and a diminished flow to the right. An explicit calculation of the flow field is obtained by solving the conservation of potential vorticity relationship

$$\frac{D}{Dt} \left(\frac{f + \zeta}{H - h} \right) = 0, \quad (2.1)$$

* Flow along or across long ridges involves aspects not relevant to this study. Interested readers could consult DEFANT (1961), HUPPERT and STERN (1974) and references therein.

where f is twice the rotation rate about the vertical, ζ is the vertical component of the relative vorticity, and the feature $h(x, y)$ stands out above a flat bottom of depth H .

For sufficiently small features the flow can go over the feature. As features of increasing size are considered, there comes a point at which somewhere in the flow field a stagnation point appears. This can be calculated to occur when the maximum height of the obstacle, say h_c , satisfies (HUPPERT, 1975)

$$h_c = cRH, \quad R = U/fL, \quad (2.2, 2.3)$$

where the Rossby number R is assumed to be small, U is the assumed constant velocity of the oncoming flow, L is a typical horizontal scale of the feature, and c is a constant dependent only on the explicit shape of the feature. For features whose maximum height exceeds that given by equation (2.2), theory predicts a closed streamline region or Taylor column (HIDE, 1961).

If the fluid is stratified, the concepts discussed above of the conservation of potential vorticity, the generation of anticyclonic vorticity over the feature, and the possibility of a closed streamline region in the flow remain. The major differences are that acting against the effects of stratification, the response decays with height with a vertical scale fL/N , where N is the local buoyancy frequency and equation (2.2) must be replaced by

$$h_c = RHg(NH/fL), \quad (2.4)$$

where the function $g(NH/fL)$ is calculated from the governing equations of motion. With uniform velocity and buoyancy frequency these are (HUPPERT, 1975)

$$\Psi_{,xx} + \Psi_{,yy} + (f/N)^2 \Psi_{,zz} = 0 \quad (2.5)$$

$$\Psi_{,z} = -N^2 h(x, y) \quad (z = 0) \quad (2.6)$$

$$\Psi_{,z} = 0 \quad (z = H) \quad (2.7)$$

$$\Psi \sim -fUy \quad (x^2 + y^2 \rightarrow \infty), \quad (2.8)$$

where Ψ is the pressure divided by a reference density after the hydrostatic contribution has been subtracted, the x -axis points downstream, and the z -axis is vertically upwards. The solution of equations (2.5) to (2.8) in terms of a Green's function $G(x, y, z; x', y')$ is

$$\Psi = -fUy + \frac{1}{2\pi} fN \int_{-\infty}^{\infty} \int_{-\infty}^{\infty} G(x, y, z; x', y') h(x', y') dx' dy' \quad (2.9)$$

and equation (2.4) is the relationship for which both

$$\Psi_x(x_0, y_0, 0) \quad \text{and} \quad \Psi_y(x_0, y_0, 0)$$

first equal zero for some (x_0, y_0) . The Green's function can be calculated by standard procedures (see, e.g., MORSE and FESHBACH, 1953) and that appropriate to the case when $h(x, y)$ is circularly symmetric is presented in HUPPERT and BRYAN (1976). For our purposes, the representation when $NH/fL \gg 1$, that is, when the water depth greatly exceeds the vertical decay scale, suffices. In this case equation (2.9) can be written as

$$\Psi = -fUy + \frac{1}{2\pi} fN \int_{-\infty}^{\infty} \int_{-\infty}^{\infty} \frac{h(x', y')}{[(x-x')^2 + (y-y')^2 + N^2 z^2 / f^2]^{3/2}} dx' dy'. \quad (2.10)$$

From equation (2.10) it is apparent that the response at any point $P(x, y, z)$ is influenced by

the entire topographic feature; the influence of all points on the feature being weighted by an appropriately scaled inverse distance of the point from P . Figure 3 presents the flow field 500 m above the bottom, obtained by numerical evaluation of equation (2.10) for a steady flow of 2.5 cm s^{-1} in the direction of 30° with uniform buoyancy frequency 10^{-3} s^{-1} . Below about 500 m a closed streamline region appears, invalidating an assumption upon which equation (2.10) is based that all streamlines originate far upstream. However, the calculated flow field above the topography is still believed to be accurate. Results from using a variable, more realistic value of N will be described in section 6.

Actual flows in the ocean are frequently not steady, however. Explicitly, the time scale of the variation, in direction or magnitude, of the incident flow may be less than the time scale for the initiation of the steady flow described above. HUPPERT and BRYAN (1976) investigated some of the phenomena associated with such time dependence by considering the following simplified model. In a layer of stratified fluid containing an isolated topographic feature the fluid is considered to be initially at rest relative to rotating axes. At a particular instant, by application of a large-scale pressure gradient, a spatially uniform current builds up to flow towards the feature. Thus some aspects of the temporal variation of the incident flow are modelled. Along with the vortex squashing of the fluid columns that go over the feature, vortex stretching occurs as the fluid initially above the feature flows off it. The stretching induces a cyclonic vorticity distribution that moves under the combined influence of the anticyclonic vorticity distribution now above the feature and the oncoming flow. HUPPERT and BRYAN (1976) showed that the topographically generated eddy, as they termed it, can either be swept downstream under the dominant influence of the oncoming flow or remain near the feature due to the dominant influence of the vorticity-vorticity interaction. Assuming that $NH/fL \gg 1$, the former type of response gives way to the latter as

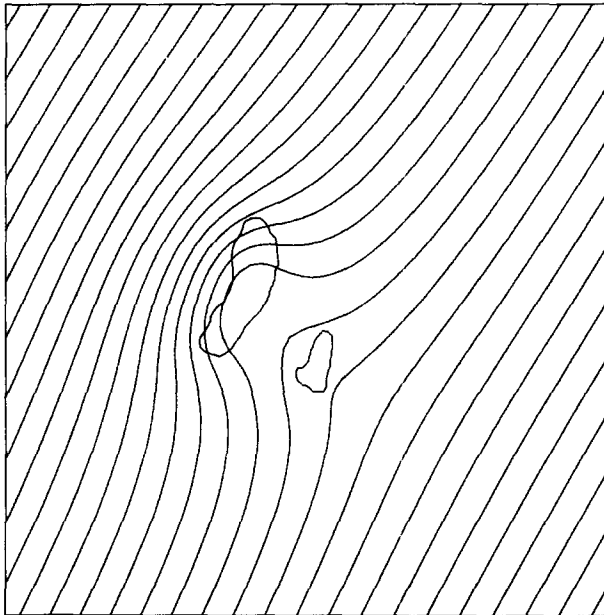


Fig. 3. Theoretical streamlines of flow over "Brontosaurus Bump" at a depth of 4800 m. Far upstream there is a steady flow of 2.5 cm s^{-1} oriented towards 30° in a fluid of buoyancy frequency 10^{-3} s^{-1} .

Nh_m/U exceeds a quantity of order 10, when h_m is the maximum value of $h(x, y)$. Figures of the flow field and resulting temperature distribution are presented by HUPPERT and BRYAN (1976), to which the reader is referred for further details.

Part of the aim of the present study was to compare the observations with the theoretical models and to determine if phenomena neglected in the models, such as tidal motions, internal waves, boundary-layer separation, or turbulence, to name just a few possibilities, were of such importance as to alter fundamentally the observed flow field.

3. NEUTRALLY BUOYANT FLOATS

Neutrally buoyant floats were used to explore the detailed spatial variability of currents in the area bounded by the outermost current meter moorings. Most floats were ballasted to settle at 4800 m, close to the top of the hill. The variations in float depths were of order ± 50 m. The design of the floats has been described by SWALLOW *et al.* (1974). Float positions were determined acoustically from an interrogator unit either towed alongside the ship at a depth of 10 m, or lowered with the CTD. The latter option enabled floats that lay in a shadow zone for interrogation from the sea surface to be tracked.

Previously, the ship and interrogator position had been determined from satellite navigation fixes and dead-reckoning using a two-component, hull-mounted ship's log. We improved on this system by using an array of three near-bottom moored float circuits as fixed acoustic beacons. The positions of the beacons were determined by least squares fitting to many satellite dead-reckoning ranges. Unfortunately, at the start of the observations the housings for the acoustic beacons were required for testing and not until later in the study were all the beacons in place. The probable errors in range fixing to the floats as indicated by range errors to the beacons were of the order of 0.1 km.

The track of a float was determined from a series of range arcs from the interrogator whose angle of cut was large enough to make adequate position fixes. Typically six to eight position lines were obtained on each float daily. From the fixes, a daily noon position was interpolated and it is these data that have been analysed. The tidal components in current meter records from 4800 m were of the order of ± 5 cm s⁻¹, implying a float excursion during a tidal cycle of ± 500 m. This is in general small compared with the mean daily motions measured by the neutrally buoyant floats, but it introduces an error into the estimation of the noon positions. Figure 4 shows the float tracks obtained during Cruise 70.

Preliminary information from mooring 187 indicated a northward flow at 5100 m immediately prior to the experiment and so the first float (float channel 2) was deployed south of the hill early on 1 April. Over the next two days, during which current meter deployments were carried out, it became clear that float 2 was not moving northwards, but was going slowly eastward and so the second float (channel 3a) was launched late on 2 April, just west of the hill. Within one day this float crossed the north end of the hill and turned towards the northeast.

The different tracks indicated the spatial inhomogeneity of the flow and floats were placed in succession around the hill (channels 8, 9a, 12, and 17 were all launched on or before 4 April). Over the next four days the floats revealed the flow to be eastward south of the hill, fast and roughly parallel to the flank of the hill on its westward side, and very slow within 10 km of the eastern flank of the hill.

As the floats moved far from the hill they were recovered and redeployed (e.g., tracks 3a, b).

Some care should be exercised in the interpretation of Fig. 4. The float tracks span three weeks and their detailed study shows that during that time there were changes in the flow pattern (for example where tracks 9a and 13 cross one another, the direction of the flow clearly changed by 45° in two weeks). Thus for a detailed analysis of flow patterns, the series of synoptic "snapshots" from combined current meter and float observations shown later in this paper are more useful. The float tracks do, however, show several well-defined features:

- (1) The flow in areas that might be expected to be unaffected by the hill appeared to have a marked curvature with a centre of circulation approximately 25 km west of the hill.
- (2) The daily mean speeds recorded by the floats furthest from the circulation centre and hopefully free from topographic influences were for the most part in the range 1.5 to 2.5 cm s^{-1} .

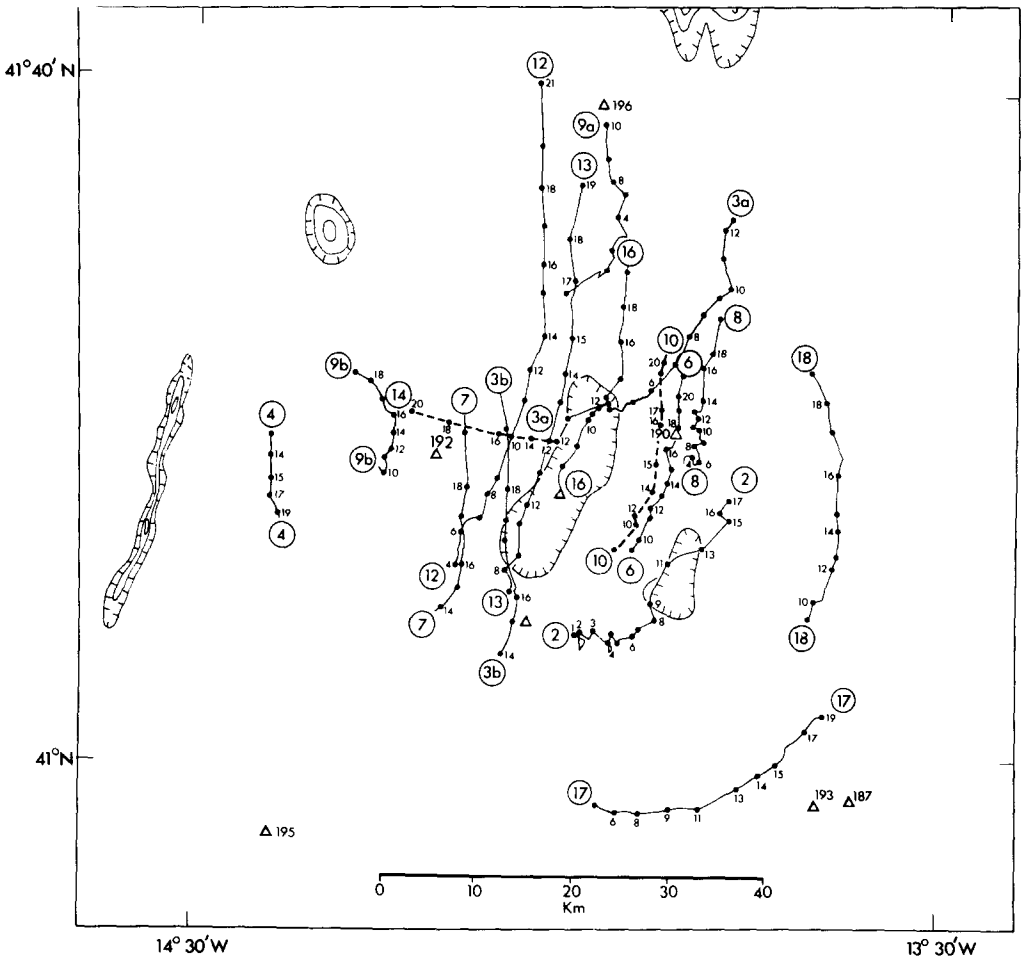


Fig. 4. Neutrally buoyant float tracks at 4800-m depth (solid lines), at 3000 m (float 10), and 500 m (float 14). Interpolated noon positions are marked on each track for days in April, 1975. The locations of other nearby topographic features are also shown as are the positions of the current meter moorings.

- (3) Speeds up to 10 km west of the westward flank of the main hill were as high as 4.5 cm s^{-1} .
- (4) Floats passing to the east of the main hill and remaining within 10 km of the centre of the topography (floats 6 and 8) had speeds in the range of 0.5 to 1.5 cm s^{-1} , significantly less than speeds west of the hill or in the far-field flow.
- (5) Two floats were launched at shallower levels. One (channel 10) at 3000 m launched at the same time and position as float 6 moved with a speed only 30% higher and deflected approximately 5° towards the west, suggesting small vertical shear between 3000 and 4800 m. A 500-m float (channel 14) launched above the western flank of the hill on 12 April moved westward at 2 cm s^{-1} , virtually at right angles to the deep flow.

The above points illustrate the understanding of the flow field that was available at the time of the observations. The curvature of the far-field flow and the temporal changes in flow direction during the observations make the interpretation of the float data alone difficult. There is undoubtedly structure on scales comparable with the horizontal dimension of the topography embedded in the far-field flow. Subsequent analyses will show approximately cross-stream sections of flow speed derived from both floats and current meters; however, float observations alone show speeds in a jet west of the hill as high as twice the estimated far-field speed and very low speeds (of the order of half the far-field speed) in a considerable area east of the hill. These results are consistent with the circulation to be expected from theoretical considerations.

The 500-m float shows the gross changes in flow patterns between the main thermocline and the deep water, and the 3000-m float shows the relatively small shears in the deep water. In hindsight, in view of the directional problems with the deep current meters (see section 4), it is unfortunate that other float levels were not used in the bottom 1000 m or so to delineate the deep-shear structure in the vicinity of the hill. Such observations are, however, difficult to make because of the acoustic shadow zones formed by the hill itself.

4. MEASUREMENTS FROM MOORED CURRENT METERS

Introduction

The current meter array shown in Fig. 2 consisted of: an outer triangle of moorings, each 40 km from the centre of the main bump; an inner triangle, with a 13-km radial spacing; and a single mooring in the centre of the pattern, directly on top of the bump. The outer triangle had current meters at 300, 1300, 2500, 4200, and 4800 m in 5340 m of water to monitor motions throughout the water column. The inner triangle measured the deep flow with instruments at 4200, 4800, and 5200 m. The lowest instruments were thus just over 100 m above the sea floor. Finally, at the central mooring, there were current meters at 3500, 4200, and 4800 m in about 5000 m of water. All moorings were supported by subsurface buoyancy.

On each mooring the 4800-m level was instrumented with vector-averaging current meters (VACM's) (AMF Electrical Products Division), which measured temperature and horizontal current velocity. Other depths carried Aanderaa instruments, and although they also recorded temperature, the resolution of *ca.* 0.02°C was too coarse to allow meaningful deep measurements. The instruments at 300 m included pressure sensors, which monitored

the vertical motion of the moorings. A 15-min sampling rate was used for all the moored instrument measurements.

All the VACM's gave complete current records. The Aanderaa meters proved problematical; compass problems due to the nickel coating on the meters nullified the value of the records from 3500 m and deeper (HENDRY and HARTLING, 1979). We will deal with the good data from 300, 1300, and 2500 m, along with the VACM records from 4800 m, which provide considerable information on the deep flow.

In discussing the current meter data, we present (Fig. 5) data from April (corresponding to *Discovery* Cruise 70) in the form of vector stick diagrams, which best illustrate the temporal behaviour of the flow. The second method of presentation (Fig. 12) combines the 4800-m measurements from moored instruments with flow vectors derived from the float tracks in maps at two-day intervals, which reveal some of the spatial structure of the deep flow. (The maps will be discussed further in section 6.) All velocity time series were filtered

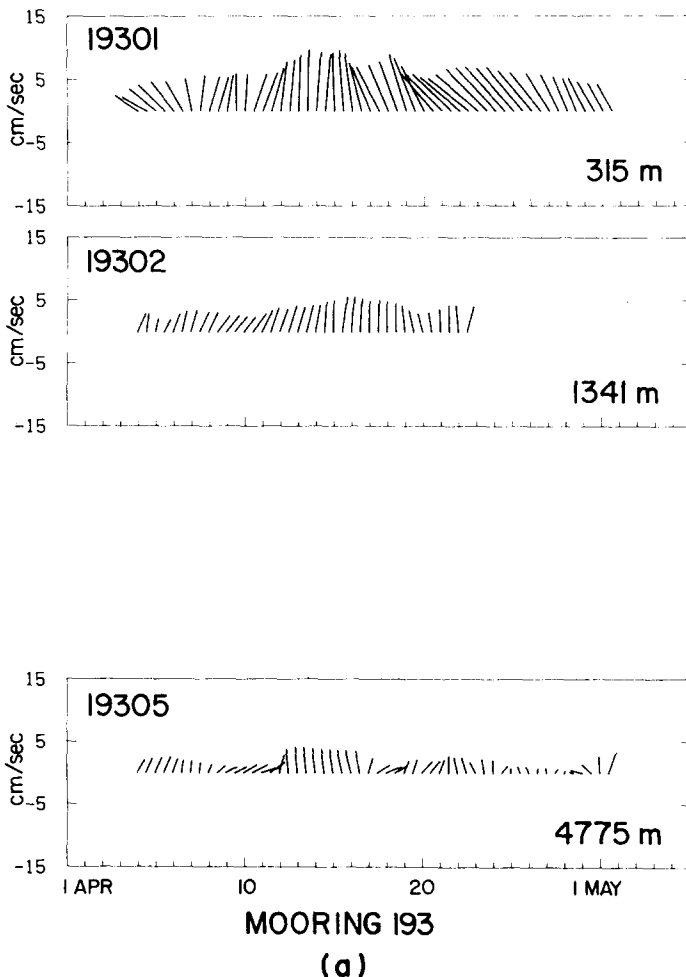


Fig. 5. (a) Vector stick diagrams of low-pass filtered horizontal current velocity from far-field mooring 193 during April, 1975. North is upward in the figures. (b) Mooring 195. (c) Mooring 196.

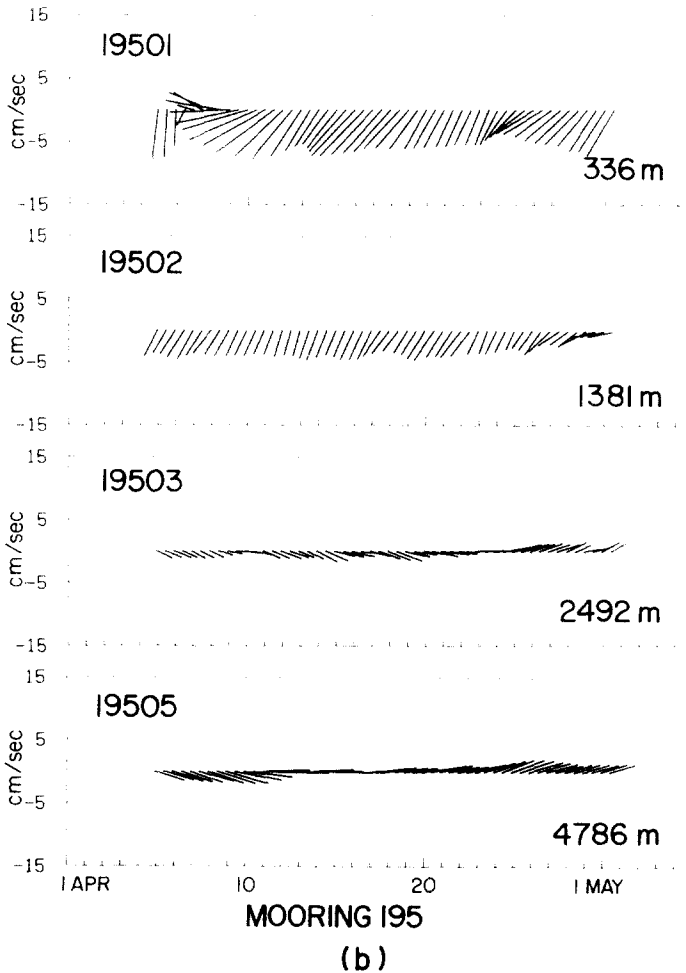


Fig. 5(b).

with a 37-h time domain half-width Gaussian low-pass filter to remove the energetic semi-diurnal tidal oscillations and inertial period motions, which were characterized by maximum speed changes of up to 10 cm s^{-1} a day at 4800 m. The filtered series are sampled at 12-h intervals in the time series presentations.

Full depth moorings

The outer triangle of moorings provides information about the vertical structure of the flow and defines the far-field currents at 4800 m. There were significant differences in vertical structure at the three outer points and these differences have some bearing on the deep-flow patterns. As seen in Fig. 5, at mooring 193, southeast of the bump, the flow had positive northward components at all levels from 300 to 4800 m, with typical speeds dropping from near 6 cm s^{-1} at the upper level to 4 cm s^{-1} at 1300 m and 2 to 3 cm s^{-1} at 4800 m. There was some temporal variation in the April flow, and in particular at 4800 m there was a relatively strong northward burst lasting from 12 to 16 April with speeds near 4 cm s^{-1} , which followed a more gradual veering of flow occupying the first eight days of

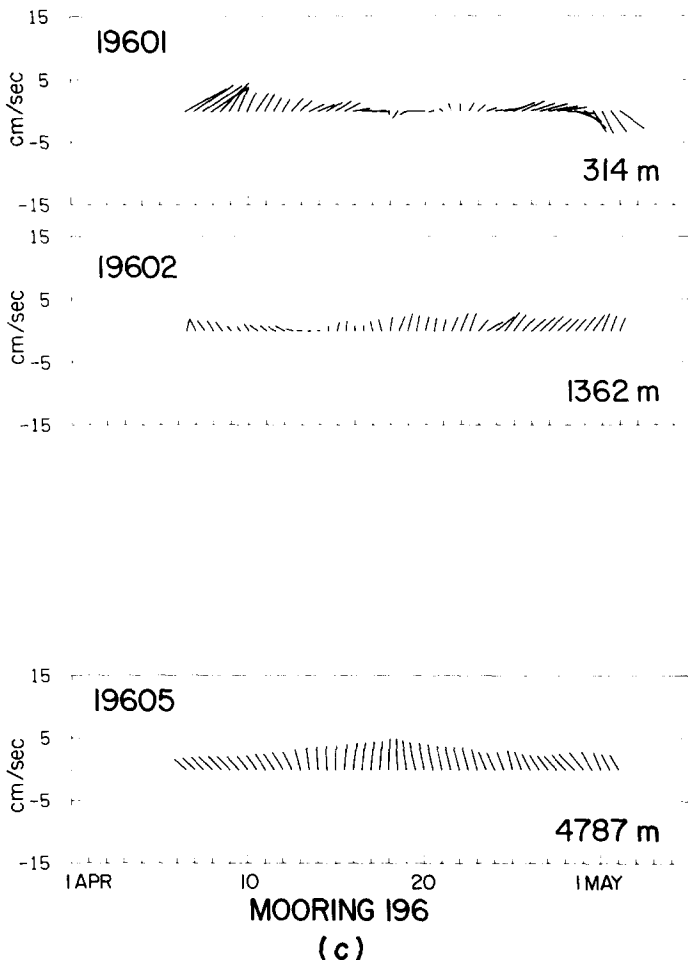


Fig. 5(c).

record. The abrupt change in flow on 12 April was likely due to the advection of spatial velocity gradients across the site of mooring 193. After this event passed, the flow looked much like that observed during the first part of the record. The velocity scale $U = 4 \text{ cm s}^{-1}$ and time scale $T = 6 \text{ days}$ define a spatial scale $UT = 21 \text{ km}$, which is similar to the internal radius of deformation in the area. Over the abyssal plain the density measurements give a calculated radius of deformation of 27 km.

At mooring 195, southwest of the bump and 58 km west of mooring 193, the vertical structure of the flow was markedly different. At 300 and 1300 m the currents from mooring 195 were generally oriented southwest, with speeds of about 7 cm s^{-1} at 300 m and 4 cm s^{-1} at 1300 m. Between 1300 and 2500 m the flow turned towards the southeast and east; then there was not much change from 2500 to 4800 m. Thus, over 58 km in horizontal separation, the deep flow changed in direction by 90° and in vertical profile the currents changed from unidirectional flow to a flow that reversed in direction. The differences in flow and flow structure between moorings 193 and 195 are examples of the mesoscale variability that is now an accepted part of ocean physics.

At mooring 196 north of the bump and 80 km from each of the southern outer moorings, there was a northward component of flow at both 1300 and 4800 m, as observed at mooring 193, with speeds of 1 to 2 cm s⁻¹ at 1300 m increasing to 4 to 5 cm s⁻¹ at the lower level. At 300 m at mooring 196, the flow was northwestward during the first half of April, but it weakened and rotated through almost two complete revolutions during mid-April. At the deepest level, which is of most interest for the study, mooring 196 showed a gradual acceleration giving maximum speeds of 5 cm s⁻¹ near 16 April and a subsequent slackening of the flow back to northwest.

There were very significant changes in flow over the scales of the outer triangle, and the changes make the mapping of the deep flow and determination of a far-field boundary condition for the study quite difficult. At 4800 m the float tracks give considerably more information but, as we shall see, even with them it is not possible to map the deep flow unambiguously. Although it could be argued that the internal radius of deformation is a natural scale for horizontal variability and sampling of the background flow, the float data show that there is structure on considerably smaller scales and with the seven moorings deployed in the study a complete mapping of the highly structured deep flow is simply not possible. In any event the study faced a spatial aliasing problem that complicates the understanding of any topographic effects on these deep currents.

Inner moorings

There was a general similarity in currents measured at 4800 m at the four inner moorings during April (Fig. 6). The flow changed from eastward or northeastward early in the month to a stronger northward flow in mid-month, and there was a further increase in speed and a veering to the northeast at the three northernmost moorings towards the end of the month.

The most noteworthy feature in the closely-spaced deep measurements was the reduction in speed at mooring 190 east of the bump, compared with the other three inner moorings. During most of April, mooring 190 consistently showed speeds of the residual current that were slower by a factor of two. Until about 16 April, the 4800-m flows at moorings 192, 194, and 197 had speeds of 2 to 3 cm s⁻¹, while at mooring 190, 14 km east of mooring 194, the speed was close to 1 cm s⁻¹. From 16 to 24 April, the deep flow accelerated to about 2 cm s⁻¹ at mooring 190 and to near 4 cm s⁻¹ at the other three inner moorings.

During the last six days of April the pattern began to change and a much stronger flow developed at mooring 194 south of the bump and at mooring 197 directly over the bump, with speeds of 7 to 10 cm s⁻¹ at the former and 5 to 7 cm s⁻¹ at the latter. At moorings 192 and 190 flanking the bump during the six days there were flows comparable at speeds of 3 to 4 cm s⁻¹ at 4800 m, and the general impression is that of a jet flowing over the bump.

The implications of these measurements are discussed in more detail in section 6, where we argue that the reduction in speed at mooring 190 is an effect of the influence of "Brontosaurus Bump" on the admittedly highly-structured background flow.

Temperature measurements from moored instruments

The VACM's at 4800 m had sufficient temperature resolution to measure the small fluctuations at that level, but the absolute calibration was inadequate to measure differences from one mooring to another in deep water. The temperature fluctuations at any mooring at 4800 m had maximum r.m.s. values of 0.006°C and the spatial average r.m.s. was 0.004°C during April, but this was mainly of high-frequency origin. The low-pass

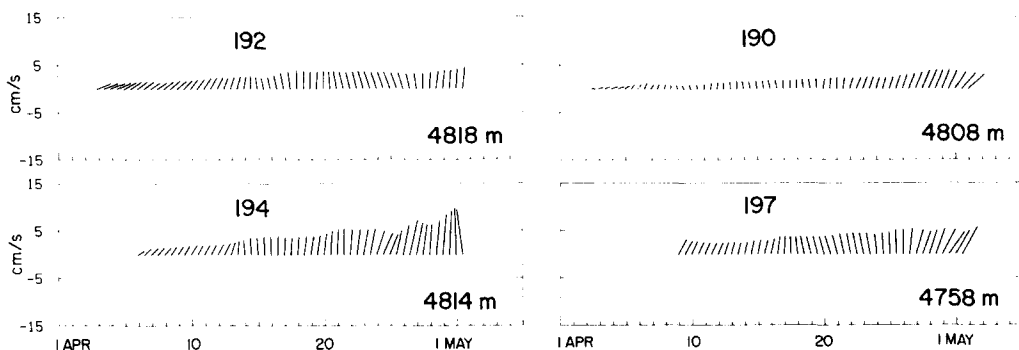


Fig. 6. Vector stick diagrams of low-pass filtered horizontal current velocity at 4800 m from mooring 197 on top of "Brontosaurus Bump" and moorings 192, 194, and 190 in the inner triangle. North is upward.

filtered temperature fluctuations anywhere at 4800 m had a maximum April range of 0.003°C with r.m.s. values of only 0.001°C . The vertical gradient of potential temperature at 4800 m was of the order 0.006°C per 100 m so internal wave isotherm displacements of 60 m were common, but during Cruise 70, the lower frequency isotherm fluctuations were of order 10 m and thus much smaller than the horizontal spatial variations during the CTD survey, as discussed in section 5.

5. THE DENSITY PROGRAM

Figure 2 shows a plan of the 12 CTD stations occupied on Cruise 70 that were used in the analysis described below. A further 19 stations were occupied during the cruise, but for the reasons already mentioned the data from them are unusable. Float-tracking requirements constrained the strategy of the hydrographic program and instrumental problems severely reduced the final data return. While hindsight shows that the goals of the experiment would have been better served by a denser CTD sampling near the bump, the data do show the topographic effects in an interesting and unambiguous way.

Instrumental considerations

The small temperature gradients at abyssal depths demand high quality instrumentation and careful calibration. The prototype Brown CTD used in the study is capable of resolving temperature differences of 0.0005°C and conductivity changes equivalent to 0.001×10^{-3} in salinity. During Cruise 70 however, the conductivity cell in the CTD deteriorated and finally failed completely. Lacking a spare cell, a fixed resistor was installed in place of the old cell and only pressure and temperature were measured on the final 12 casts during the period 12 to 18 April. The conductivity channel apparently also affected the temperature channel and extensive temperature intercalibrations with the rosette multisampler proved to be necessary. Although individual reversing thermometer readings lack the high resolution of the CTD, averages over many intercomparisons define the CTD temperature calibration to within a few thousandths of a degree. The reversing thermometers used in the study were subsequently carefully recalibrated by Mr JOHN MOOREY at I.O.S. Wormley and the final result was an excellent set of CTD-rosette temperature intercomparisons.

There was a change in temperature calibration of the CTD by about 0.01°C when the conductivity cell was replaced, as was determined by averaging over Stas 8823 to 8839

occupied with the failing conductivity cell and Stas 8842 to 8853 with the replacement resistor. The temperatures from Stas 8840 and 8841 are completely unusable. Initially we considered treating the two groups 8823 to 8839 and 8842 to 8853 together by correcting the two sets of temperatures with constant offsets, but there was evidence of a further calibration discrepancy among stations of the first group, apparently developing in parallel with the deteriorating conductivity cell and amounting to temperature offsets of up to 0.006 °C. The reversing thermometer readings were not precise enough to correct individual stations and faced with the doubtful readings from the first group of stations the final decision was to treat only the second group in which we had full confidence.

Of the 31 CTD stations during Cruise 70, we thus can rely quantitatively only on the results from the 12 from the latter part of April, which were made with the fixed resistor replacing the conductivity cell. These include Sta. 8842 directly on top of the bump and Stas 8843 to 8853 over the surrounding abyssal plain. Among Stas 8842 to 8853 a total of 32 rosette multisampler calibration points (each involving an average of two reversing thermometer readings) were taken at depths greater than 4000 m where the spatial temperature gradients are weak. The data defined the absolute calibration offset of the CTD over the 12 stations to be -0.024 ± 0.001 °C, with the error limits being the standard error of the mean. There was no evidence for calibration changes during the latter stations: the mean offset defined for the 14 calibration points at Stas 8842 to 8847 agreed to within 0.001 °C with the offset similarly defined by averaging over 18 calibration points at Stas 8848 to 8853. The main outcome of our calibration procedures is that the measurements finally selected for analysis should be highly reliable.

No conductivity measurements were made during Cruise 70, so we combined the observed temperatures with a temperature-salinity relationship to define salinities and this allowed the calculation of density and other derived quantities. Reversing thermometer readings and salinity samples taken on both cruises were combined with the CTD measurements from Cruise 72 to produce a refined local definition of the known potential temperature (θ -salinity (θ -S) relationship in the eastern basin of the North Atlantic (WORTHINGTON and METCALF, 1961). From this relationship a polynomial was derived for salinity as a function of potential temperature between 2 and 3.8 °C, the latter temperature corresponding to approximately 2000 m, the upper limit of North Atlantic Deep Water. The r.m.s. difference of salinity from the derived θ -S curve and CTD salinities from Cruise 72 was of the order of 0.002×10^{-3} for 1-dbar averages over the given potential temperature range. This is comparable to the noise levels of the CTD alone; no departure from an exact θ -S relationship is detectable. Above 2000 m there is a considerable scatter in the θ -S relationship because of intermixing of North Atlantic Central Water and more saline water from the Mediterranean Sea outflow, and we restricted our analysis to the deeper levels.

Topographic effects

The Cruise 70 CTD data immediately made it clear that there was a strong temperature signal in the deep water associated with "Brontosaurus Bump". At 4800 dbar the water over the bump was colder by about 0.01 °C than water at this pressure level at far-field stations. The signal represents vertical excursions of hundreds of metres in the weakly stratified deep layers. The cold water over the bump was seen in the first group of CTD stations as well as in the final group. Station 8834 in the first group was on top of the bump only 1 km from the later Sta. 8842 and, in spite of the calibration difficulties discussed above, a similar cooling by about 0.01 °C at 4800 dbar was evident at Sta. 8834 relative to

the far-field average among the earlier stations. However, we will deal quantitatively only with Stas 8842 to 8853.

As a preliminary description we present in Fig. 7 histograms of the distribution of potential temperatures among the later stations at four deep pressure levels. The values are smoothed in the vertical over 25 dbar. At 5000 dbar the potential temperature at Sta. 8842 of 2.062°C was between 0.007 and 0.010°C colder than at any of the 11 far-field stations, including Sta. 8845, which is only 5 km from Sta. 8842 on the plain east of the bump. Similarly, at 4800 and 4500 dbar water over the bump was colder than at any of the far-field stations. At 4200 dbar, however, three of the far-field stations were colder than Sta. 8842, and the scatter amongst the various stations was increasing noticeably. The nearly uniform temperatures at the deepest levels at far-field stations show that the topographic adjustment is very localized horizontally and no horizontal mapping is possible with the data, but we can examine the vertical structure of the temperature anomaly over the bump.

The potential temperature anomaly at Sta. 8842 relative to the average among all 11 far-field stations is shown in Fig. 8. The variability in the far field is described by the 1 S.D. error bars in the figure. The cold anomaly at Sta. 8842 is clearly evident up to about 4200 dbar, above which level the bump station generally is less than 1 S.D. different from the mean far field. The background temperature variability increases greatly at higher levels where the vertical temperature gradients are greater.

On the assumption that the flow was steady and adiabatic, and that the potential temperature was constant on streamlines, we can deduce the vertical excursion undergone by the water overlying the bump. The minimum potential temperature at Sta. 8842 of 2.062°C at 5025 dbar is as cold as found at the bottom over the plain, where the minimum potential temperatures ranged between 2.059 and 2.064°C . This is consistent with the idea that the water over the bump originated near the ocean floor some 450 m below the summit of the bump.

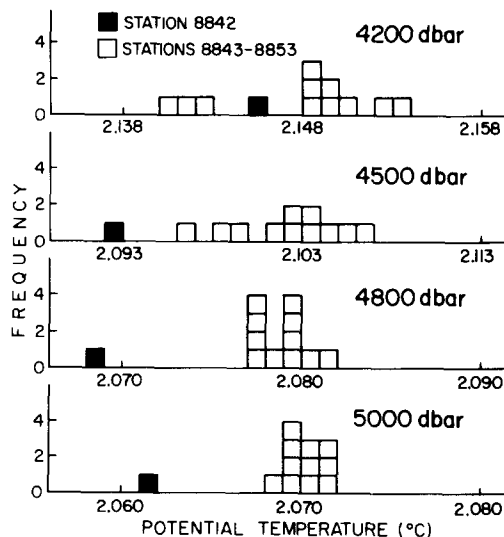


Fig. 7. Histograms showing the distribution of potential temperature at pressure levels between 5000 and 4200 dbar for Sta. 8842 on top of "Brontosaurus Bump" and 11 far-field stations.

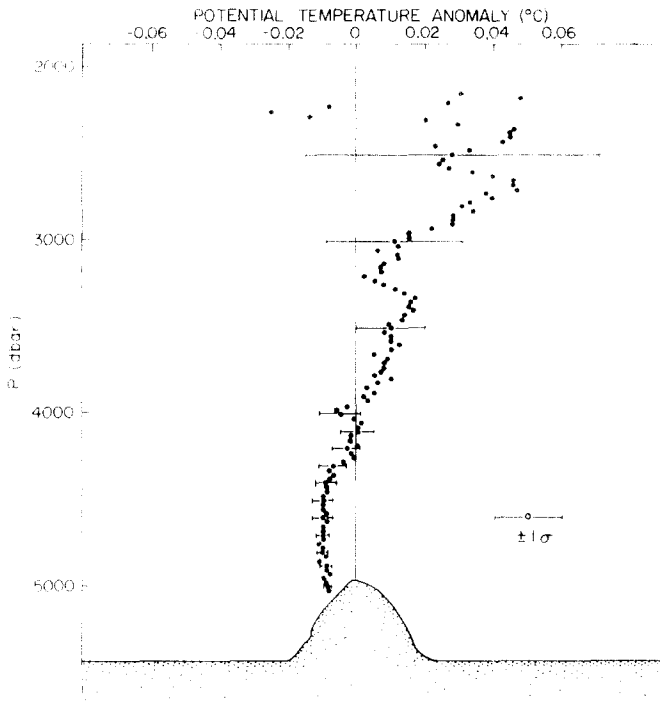


Fig. 8. Potential temperature anomaly vs pressure level at Sta. 8842 relative to the mean among 11 far-field stations. The error bars give the r.m.s. far-field temperature fluctuations at selected levels.

We defined a mean far-field potential temperature profile $\bar{\theta}(p)$ by averaging over the 10 deepest far-field stations that reached 5375 dbar. (Station 8850 ended several hundred dbar shallower than the others.) The vertical excursion undergone by a fluid parcel over the bump with a potential temperature θ at a pressure level p is thus given by $p_0 - p$, where p_0 is the far-field original pressure level of the parcel defined by $\bar{\theta}(p_0) = \theta(p)$. Figure 9 presents $p_0 - p$ as a function of the far-field pressure level p_0 . Error bars on displacement shown in the figure are the r.m.s. isotherm depth fluctuation among the 10 far-field stations at level p_0 , defined by dividing the r.m.s. potential temperature fluctuation by the mean vertical potential temperature gradient

$$(d\bar{\theta}/dp)_{p=p_0}.$$

The inferred vertical displacement over the bump is striking, with values of from about 350 dbar on surfaces originating near the ocean floor decreasing to zero at 4100 dbar. At the latter level the topographic effects have faded into the far-field r.m.s. noise level of about 30 dbar. The noise in displacement is much more stationary in the vertical than the noise in temperature. At the very deepest levels below 5200 dbar there is an increase in isotherm depth variability in the far field that is related to the spatially variable well-mixed bottom layers.

Figure 10 is a vertical profile of the dynamic height anomaly at Sta. 8842 relative to the background. This is defined by

$$\Delta D = \int_{p_0}^p (\delta - \bar{\delta}) dp', \quad (5.1)$$

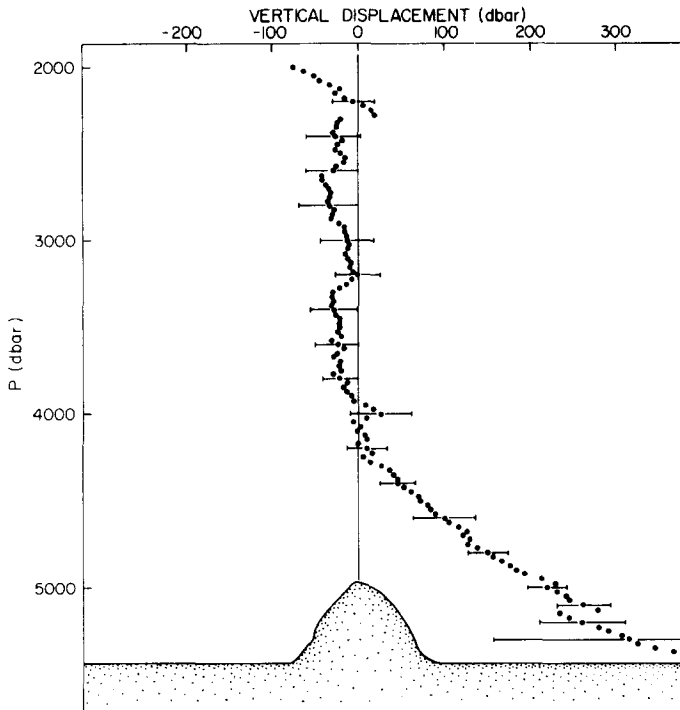


Fig. 9. Inferred vertical excursion from far-field level undergone by water parcels above the bump at Sta. 8842 as a function of inferred original far-field level. The error bars are r.m.s. isotherm depth fluctuations among the 10 deepest far-field stations.

where δ is the specific volume anomaly at Sta. 8842 and $\bar{\delta}$ the average among the 11 other stations. To show the perturbation associated with the deep density anomaly, we have chosen a reference level $p_0 = 4100$ dbar, which is the nominal level at which the topographic effect vanishes. There is a transition between 3900 and 4200 dbar where there is essentially no vertical variation in the dynamic height anomaly, and the bottom value of the anomaly is insensitive to changes in the choice of reference level by ± 250 dbar. The colder and denser water over the bump gives an increasing dynamic height deficit (equivalent to a high pressure anomaly) as the pressure increases to 5025 dbar. The increasingly large signal in dynamic height at levels above 3800 dbar is part of the mesoscale variability that contributes to the horizontal current shear observed at 4800 m in the float tracks and moored current measurements. The error bars in Fig. 10 are the r.m.s. fluctuations of dynamic height relative to 4100 dbar for far-field stations. At 5025 dbar the topographic effects stand out from the far-field variability by over 3 S.D. The dynamic height signal at Sta. 8842 above 4100 dbar is typical of the other stations: the water above 4100 dbar over the bump is about 1 S.D. warmer than the average far-field stations, as seen in Fig. 8, and the dynamic height mirrors this behaviour.

The maximum dynamic height anomaly at the deepest level of -0.0009 dynamic metres can be used to estimate the horizontal currents associated with the topographic effects. With the assumption of geostrophy, the horizontal flow associated with the dynamic height variation is

$$\mathbf{u} = [\mathbf{k} \wedge \nabla(\Delta D)]/f, \quad (5.2)$$

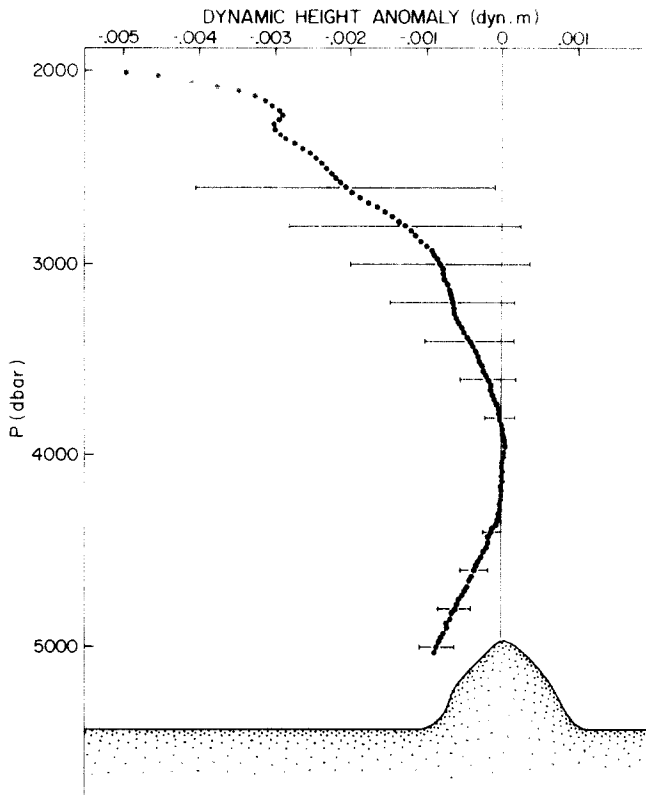


Fig. 10. Dynamic height anomaly at Sta. 8842 relative to the far field, referred to 4100 dbar. The relatively low dynamic height at 5000 dbar at Sta. 8842 is equivalent to a high pressure anomaly there.

where \mathbf{k} is the vertical unit vector. We have no definite information on the horizontal gradients of dynamic height over the bump, but the far-field station closest to Sta. 8842 was only 5 km removed. Using 5 km as a horizontal scale we derive a flow perturbation of 1.9 cm s^{-1} at the 5025-dbar level relative to the flow at 4100 dbar. If the horizontal scale is less than 5 km the local flow perturbation is accordingly greater.

Because the topographic effects can be most easily visualized in terms of vortex stretching, it is interesting to estimate the relative vorticity introduced into the water above the bump by the topography. For frictionless, non-diffusive flow, Ertel's theorem indicates that the potential vorticity in a stratified fluid

$$P = (2\mathbf{\Omega} + \zeta) \cdot \nabla \rho \quad (5.3)$$

is conserved along streamlines, where $\mathbf{\Omega}$ is the Earth's rotation vector, $\zeta = \nabla \wedge \bar{\mathbf{u}}$ the relative vorticity of the total flow field $\bar{\mathbf{u}}$ in a frame of reference rotating with the Earth, ρ the potential density, and ∇ the three-dimensional gradient operator. A further assumption that the horizontal gradients of density are negligible compared to the vertical gradients gives $P = (f + \zeta_3)(d\rho/dz)$ where $f = 2|\mathbf{\Omega}|\sin \phi$ is the Coriolis parameter at latitude ϕ and ζ_3

is the vertical component of relative vorticity. Finally, assuming that $\zeta_3 \ll f$ and $\rho = \bar{\rho}(z)$ in the far field, the vertical component of relative vorticity on a streamline originating at $z = z_0$ in the far field is given by

$$(f + \zeta_3) \frac{d\rho}{dz} = f \left(\frac{d\bar{\rho}}{dz} \right)_{z=z_0} \quad (5.4)$$

or

$$\zeta_3 = f \left[\left(\frac{d\bar{\rho}}{dz} \right)_{z_0} / \left(\frac{d\rho}{dz} \right) - 1 \right]. \quad (5.5)$$

Note that we have neglected the spatial variation of f , which we will justify *a posteriori*.

In analysing the data we assumed that ρ varied linearly with potential temperature (including a linear variation with salinity implicitly through the θ -S relationship) and evaluated the expression

$$\left[\left(\frac{d\bar{\theta}}{dz} \right)_{z_0} / \left(\frac{d\theta}{dz} \right) - 1 \right]$$

as a function of the far-field pressure level p_0 . The resulting profile of ζ_3 can then be presented as a function of the pressure level attained by a streamline over the bump (Fig. 11). Here $d\theta/dp$ is the vertical gradient at Sta. 8842 at the pressure level defined by $\theta(p) = \bar{\theta}(p_0)$. Vertical gradients were estimated by centred differences over 150 dbar to provide smoothing, and the bump pressure levels and vertical gradients were obtained as needed by linear interpolation between standard pressure levels separated by 25 dbar.

The results of this calculation are presented in Fig. 11, which gives a strong indication of the production of anticyclonic (negative) relative vorticity by the topography. The error bars given in the figure are the r.m.s. value of $[(d\bar{\theta}/dp)/(d\theta/dp) - 1]$ at each pressure level for $d\theta/dp$ values from the 10 near-bottom far-field stations. The anomaly in relative vorticity at Sta. 8842 below 4100 dbar defined by this analysis is quite significantly different from zero as determined by the random fluctuations in the far field. The estimates of relative vorticity decrease from near $-0.4 f$ at $p = 4780$ dbar ($p_0 = 5000$ dbar in the far field) to values generally not significantly different from zero above 4100 dbar. The relatively smooth vertical variation of the vorticity calculations below 4100 dbar over scales larger than the 150-dbar smoothing scale is notable. The locally large value of relative vorticity over the bump could be roughly calculated as the result of shrinking a column of water occupying the 1240-m interval between 4100 m and the 5340-m bottom depth into a column only 770 m thick between 4100 m and the 4870-m bump summit. We note that the average relative vorticity within a 5-km radius of the bump, characterized by the measured geostrophic shear or the swirl speeds from nearby float and moored current meters, is an order of magnitude less than the local value on top of the bump.

The maximum north-south separation between any of the CTD stations was less than 80 km, giving a fractional change in f of only 0.014. The changes in total vorticity due to meridional motion over these scales are much less than the vorticity signal in the deep water at Sta. 8842 and are safely neglected in the vorticity calculation.

There is an interesting indication of a reduction in magnitude of the induced relative vorticity on streamlines originating at pressures greater than 5000 dbar in the far field, when compared to streamlines originating just above the summit of the bump. The decrease

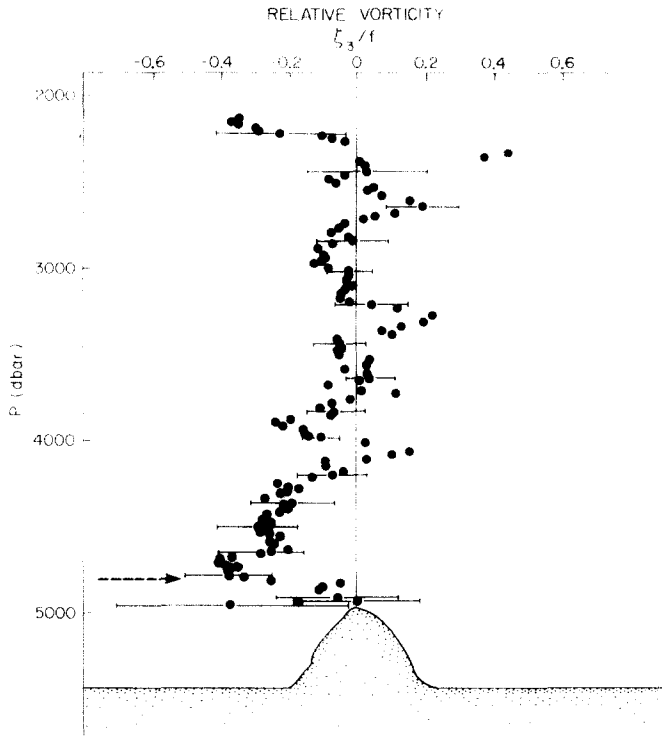


Fig. 11. Inferred relative vorticity at Sta. 8842 induced by compression of vortex lines in the flow over "Brontosaurus Bump" as a function of pressure level. The arrow at about 4800 dbar marks the flow streamline over the bump that originated in the far field at the bump summit height.

was determined to be a result of decreased vertical temperature gradients at the deepest levels over the bump rather than any marked change in the far-field vertical temperature gradients at the deeper levels. This apparent decrease in relative vorticity may be related to the finite height of the obstacle and the resulting horizontal diversion of the flow around the bump. These three-dimensional effects might result in decreased vertical vortex stretching at levels where there is a tendency for the flow to go around the bump.

The results presented in this section will be compared to theoretical modelling results in the next section.

6. SYNTHESIS OF RESULTS

We have studied the individual data sets collected during the field phase of the experiment and have presented the theoretical background. We now look at the interrelations of the observations and the degree of agreement between the observations and theoretical predictions.

(a) *The combination of float and current meter observations*

The two independent sets of velocity observations at 4800 m, from neutrally buoyant floats and vector-averaging current meters, have been combined to produce a series of "snapshots" of the 2-day mean flow field at 2-daily intervals. These are shown in Fig. 12 for

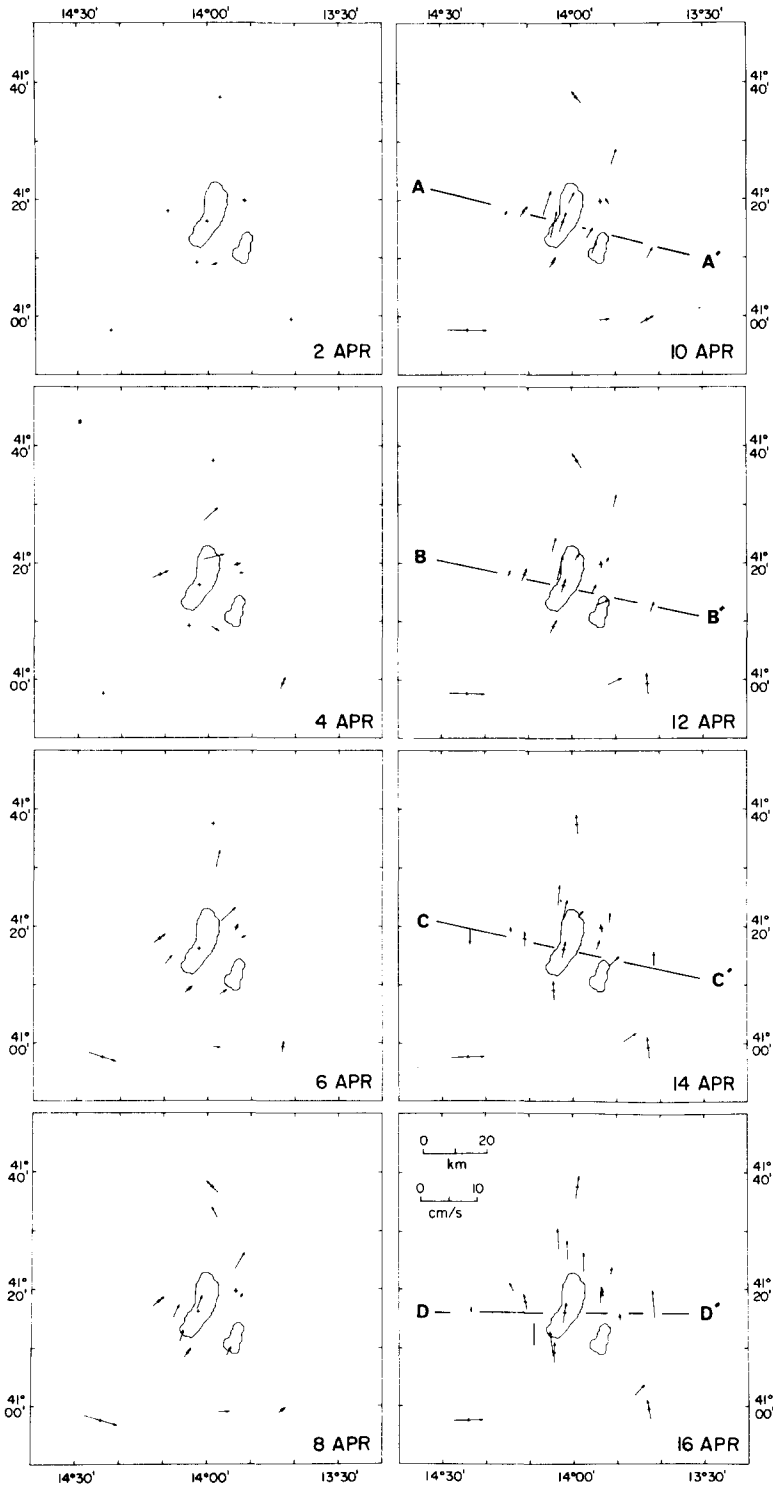


Fig. 12. Flow vectors at 4800 m from combined float tracks and low-pass filtered current meter data, at 2-day intervals from 2 to 24 April, 1975. The scales of the velocity vectors and base chart are such that the vectors also give horizontal displacement over a time interval of 2 days. Cross sections A-A' to E-E' are explained in Fig. 13.

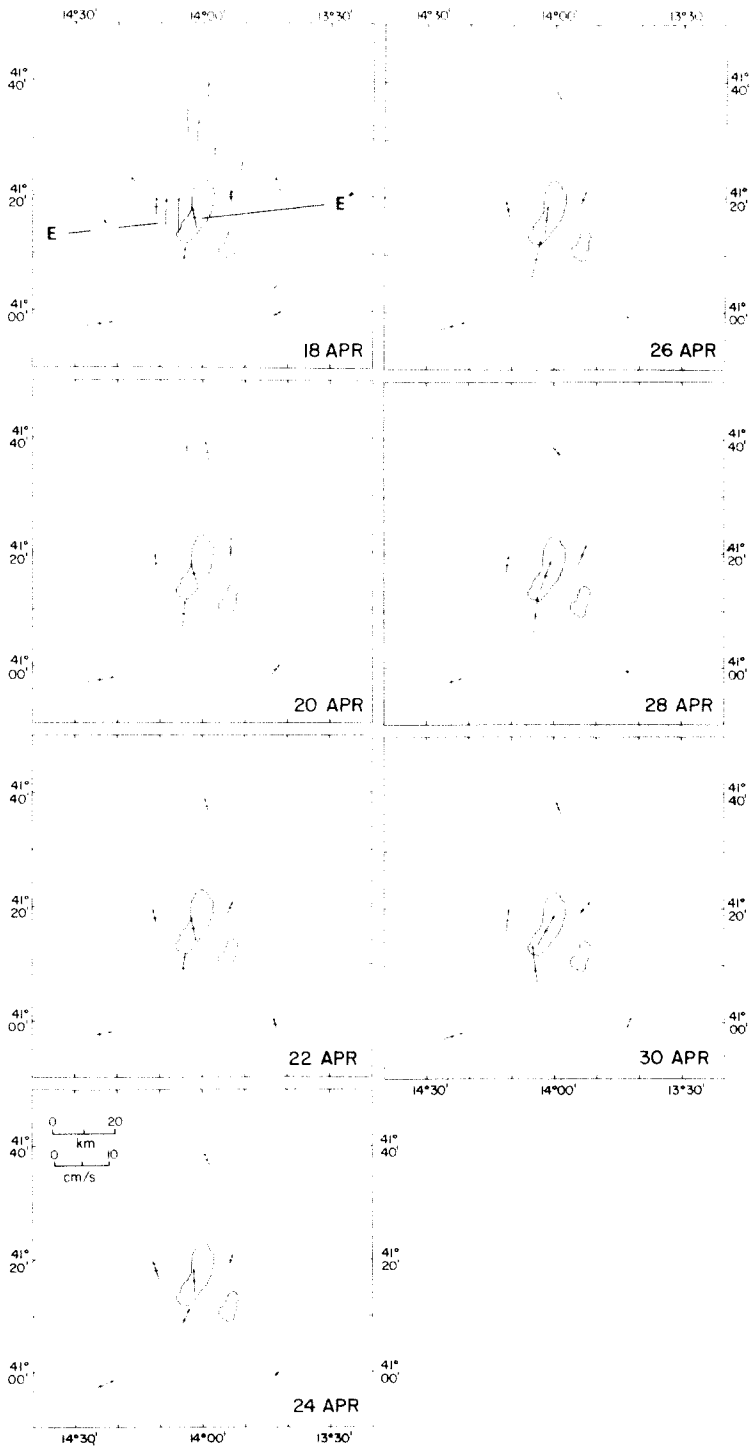


Fig. 12—continued.

2 to 30 April. The number of current vectors is small at the start and end of the period but towards the middle of the month the maps have a dozen or more observations around the hill.

The curvature of the flow field is well defined and is particularly obvious in the vectors from the outer triangle of moorings. It is best seen in the data between 8 and 18 April. A picture emerges of a centre of rotation approximately 30 km west of the bump, and it is clear that the impressed flow is far from an ideal uniform, unidirectional one.

On the assumption that the centre of curvature of the flow field remains fixed over the period of the experiment and that the main component of flow is approximately parallel to the major axis of the bump, cross-sections of the flow field have been constructed. Sections A–A' to E–E' in Fig. 12 give insight into the cross-stream structure of the flow field near the hill. (The orientations of the sections were chosen to maximize the number of current vectors on each section and to keep the angle of cut close to 90° to the local flow field.)

All the sections show the highest speeds (Fig. 13) near to the hill within 10 km of its western flank. The influence of the blocking of flow upstream of the section may be significant on section E–E' and the extent of the block has been indicated in the figure. The inadequacy of the cross-stream profiles, even on the days with the densest coverage, when there are as many as 20 independent velocity observations around the hill, is clear. However, it is obvious that speeds are persistently high west of the bump and low in the zone between “Brontosaurus Bump” and “Webb’s Foot”. This shear has already been remarked upon in the results of the current meters and the floats separately.

On sections A to D the velocity difference across the main hill was $\sim 2 \text{ cm s}^{-1}$ but by section E this increased to almost 5 cm s^{-1} . A possible explanation of this could be that the zone of high speeds is very narrow and that only in case E does a float enter the core of the jet. However the speeds well away from the hill appear to be higher on section E than those on previous sections so it may be that the higher shear is as a result of general increase in

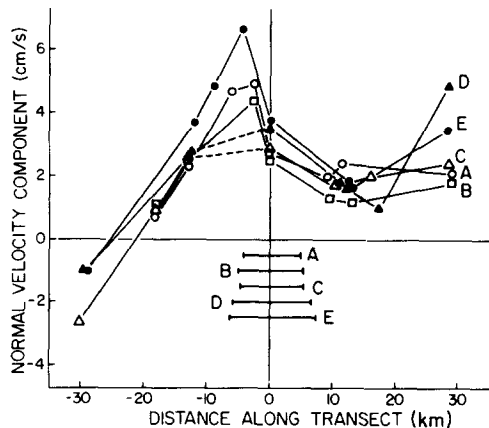


Fig. 13. Flow components at 4800 m normal to nearly east–west transects across “Brontosaurus Bump” extracted from the vector maps in Fig. 12 for 10 April (section A, flow direction 014°T), 12 April (section B, 011°T), 14 April (section C, 011°T), 16 April (section D, 000°T), and 18 April (section E, 354°T). The orientations were chosen to maximize the number of observation points on the sections and keep the angle of cut close to 90°. The projections of “Brontosaurus Bump” on the chosen transects are indicated by the bars accompanying the figure. The dashed lines included in parts of sections C and D emphasize the lack of flow data in the key region between moorings 192 and 197 during the period 14 to 16 April.

the strength of the flow between 16 and 18 April. There is evidence to support this conjecture from the data from mooring 192 (Fig. 6).

In sections A and B there is evidence that velocities over the centre of the hill are lower than those on the western flank. The validity of this observation is dependent on the comparison of float and current meter observations being valid to better than 1 cm s^{-1} in the speed range 2.5 to 4 cm s^{-1} . Previous float-VACM comparisons in the MODE-1 experiment (SWALLOW, 1977) showed r.m.s. differences of the order of 0.3 cm s^{-1} between the two types of measurement on the occasions of close passes of floats by current meter moorings. This suggests that the detailed structure observed over the bump is genuine.

(b) *Comparison of CTD observations with current measurements*

The much sparser set of CTD observations (Fig. 2) around the hill make the determination of the topographic signature in the density data more difficult than in the velocity observations; in particular, from the data set little can be said about the horizontal structure of the induced topographic effects. However, a single station (8842) over the peak of the hill serves for comparisons with the 10 or so far-field observations. The main results of the density observations were detailed in section 5. They show an implied geostrophic signal of the order of 2 cm s^{-1} across a 5-km separation between Sta. 8842 and the nearest station showing no detectable topographic influence. The figure agrees quite closely with the observed shears near the hill from floats and current meters. The geostrophic shear between the two hydrographic stations ($0.4 \text{ cm s}^{-1} \text{ km}^{-1}$) is fairly comparable to the measured shear in the currents in Fig. 13 (sections E and B on the western flank of the hill). The geostrophic computation is for the eastward slope of the topography but in that region of the flow the smallest separation between adjacent current measurements is about 20 km and this may be too great a distance for the comparison to be valid.

(c) *Comparisons between the theoretical model and the density data*

A difficulty in applying the theory of section 2 to the observations is the vertical variation of stratification. We can incorporate this variation in an approximate way in the analysis by assuming that N is a slowly-varying function of depth and using a WKB solution. This involves replacing the variable z by the scaled vertical variable z^* defined by

$$z^* = f^{-1} \int_{\text{bottom}}^z N(z') dz'$$

and using N_B , the value of N at the bottom of the water column, for N wherever it appears as a multiplicative constant in equations (2.9) and (2.10). The performance of such a procedure using the digitized bottom topography of "Brontosaurus Bump" with a grid spacing of about 0.7 km and a representative value of $N_B = 2.1 \times 10^{-4} \text{ s}^{-1}$, leads to the pressure, density, and vorticity perturbations at the position of CTD Sta. 8842 on top of the bump presented in Figs 14, 15, and 16. Below about 4000 dbar the vertical variation of pressure of the calculation is quite similar to that in the data. For example, the increasing pressure anomaly from 4100 to 5000 dbar is 0.0012 dbar, comparable to the difference of 0.0009 dyn m in the data (Fig. 10). Above about 4000 dbar variations due to non-topographic effects become important and are hence not predicted by the model calculation. There is also good agreement between the calculated and measured density fields: the model predicts a density perturbation $\delta\rho/\rho_0 \approx 1.55 \times 10^{-6}$ at 5000 dbar, which is

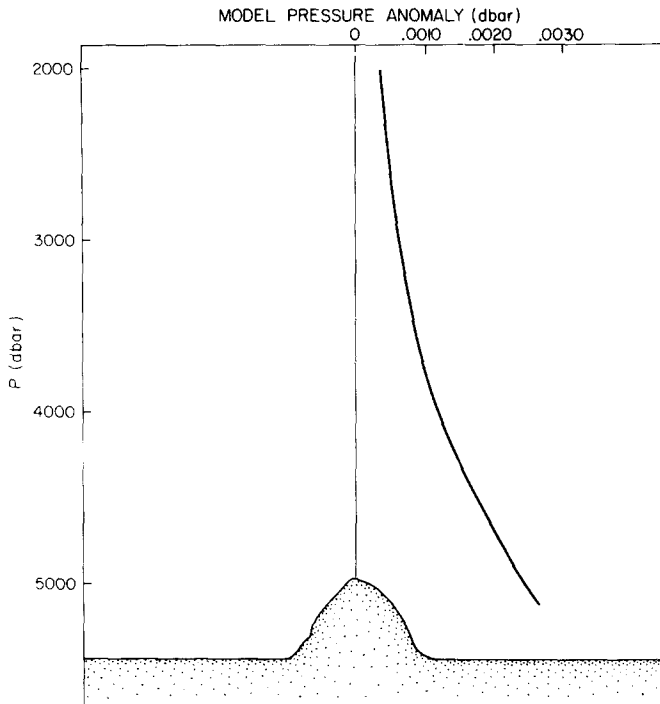


Fig. 14. Model pressure anomaly at the position of Sta. 8842. The increase in pressure anomaly in the model calculation between 4100 and 5000 dbar can be compared to the increasing dynamic height deficit in that depth range at Sta. 8842 shown in Fig. 10. (1 dbar pressure anomaly is nearly equivalent to 1 dyn m in dynamic height anomaly).

to be compared with the observed value at that depth at Sta. 8842 of 1.2×10^{-6} . The predictions of the model for the relative vorticity, shown in Fig. 16, can be compared with Fig. 11, which presents the estimates obtained from the use of Ertel's theorem on the data to evaluate the relative vorticity. Between 4800 and 4200 dbar there is a strong resemblance in shape between the two figures, though the model calculation is about 50% less than the empirical one. We conclude that the model provides a reasonable description of the topographic effects measured during the experiment.

(d) *Comparison of theory with the observed current field*

At the 4800-m level, the moored current meters and neutrally buoyant floats gathered considerable information on the horizontal currents. The result was a picture of a highly structured and evolving flow field superimposed on some topographic influences; for example, floats accelerated while passing near the western flank of the bump. From the theoretical model described above, the calculated perturbation flow field at about 4800 m at the seven fixed mooring positions is presented in Fig. 17. At all points except mooring 197 on top of the bump, the predicted flow perturbation has speeds of less than 1 cm s^{-1} . There is a difference in current of 2.0 cm s^{-1} between moorings 197 and 192, with southward flow at 192 relative to 197; this would account for the low speeds observed at mooring 192 and at nearby float positions for the first part of April. The scale of the inner mooring array was unfortunately too large to resolve the details of the flow around the topography. In Fig. 18 we present a transect of the calculated flow along the line oriented

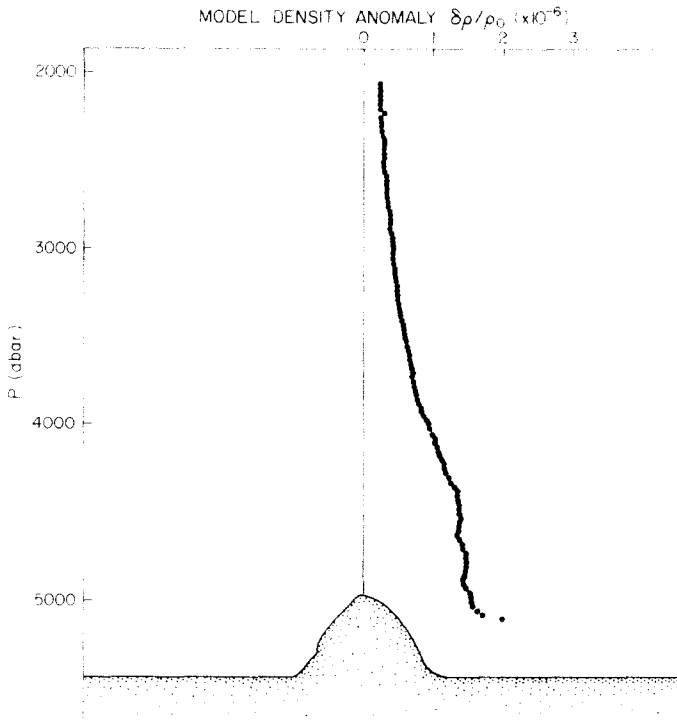


Fig. 15. Model density anomaly at the position of Sta. 8842. At 5000 dbar the density anomaly is equivalent to a temperature anomaly of about $-0.011\text{ }^{\circ}\text{C}$, and the shape of the density anomaly can be compared with Fig. 8.

to 030°T and passing through the bump centre, again at a depth of about 4800 m. Maximum speeds of 3 cm s^{-1} are predicted, with an abrupt reversal in direction from north to southwest in passing from the western side of the bump to the eastern side. Flow perturbations in excess of 1 cm s^{-1} are confined to about 7 km on either side of the bump axis along the transect.

In the flow data there are instances of flow structure on the western flank of the bump that show topographic effects. For example, on 10 April (Fig. 12) float 13 gives a 2-day average speed of 4.9 cm s^{-1} at about 3 km west of mooring 197 on top of the bump where the mean speed was 2.8 cm s^{-1} . Float 12, 4 km further to the west, had a speed of 4.7 cm s^{-1} , while at mooring 197 the speed of the mean flow over this period was 2.5 cm s^{-1} . The acceleration of the two floats passing between the moorings was about as predicted by the model. Similar occurrences of faster flow over the western flank of the bump were seen on 12 April (float 13) and 18 April (floats 3 and 7). In each case the floats moved about 2 to 3 cm s^{-1} faster towards the north than the currents at the flanking pair of moored instruments. Thus the model calculations of the flow perturbations due to the topography are consistent with these features of the observed flow at 4800 m.

7. SUMMARY AND CONCLUSIONS

Observations have been made of the flow field and density structure surrounding a small isolated hill $20 \times 5\text{ km} \times 500\text{ m}$ on an otherwise flat abyssal plain. The results of the

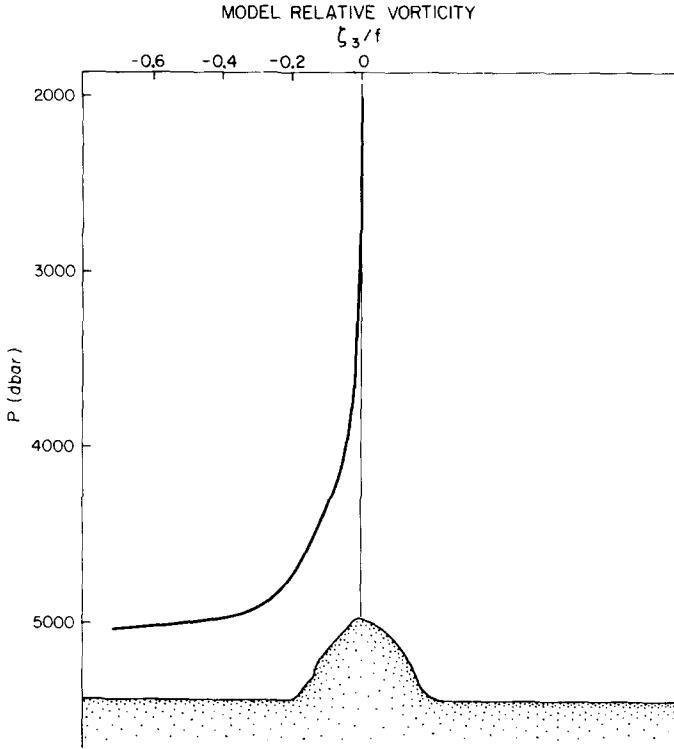


Fig. 16. Model relative vorticity calculated at the position of Sta. 8842. This can be compared directly with Fig. 11.

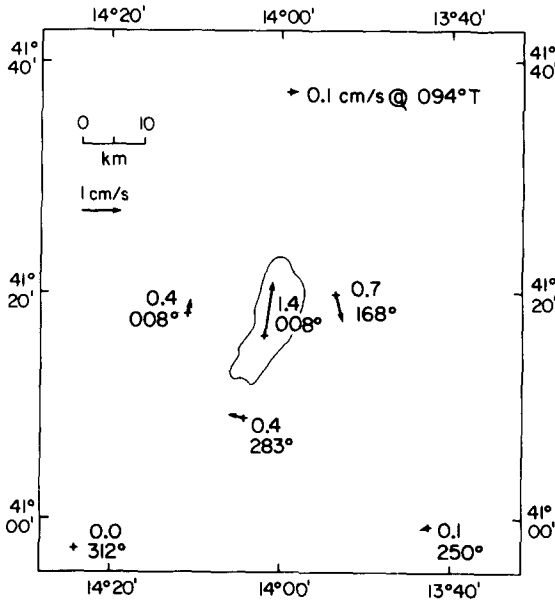


Fig. 17. Model calculations of the horizontal flow perturbations due to a topographic vortex in the geometry of "Brontosaurus Bump" at 4800-m depth and at positions corresponding to the fixed moorings in the topographic experiment.

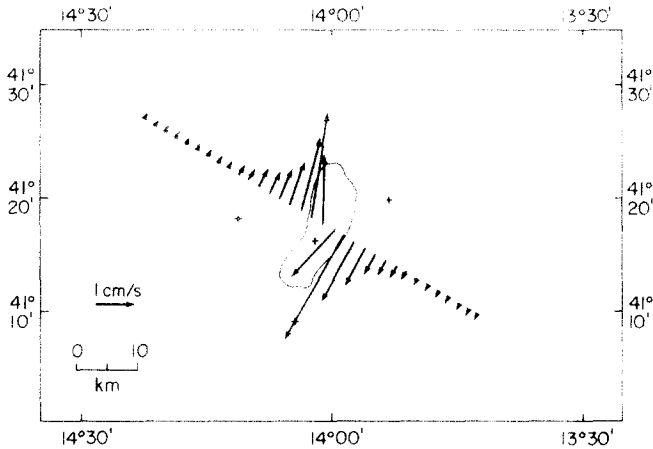


Fig. 18. Model calculations of the horizontal flow perturbations due to the topographic vortex at 4800 m along a transect over "Brontosaurus Bump" oriented normal to 030 T.

observations have been compared with a theoretical model of the flow disturbance due to such a hill.

The flow field measured by neutrally buoyant floats and current meters at a level close to the top of the hill had a radius of curvature of almost 50 km and impinged on the topography from the south. Typical speeds far from the topography were of the order of 2.5 cm s^{-1} at the level of the hill top. Near the hill the flow at this level was accelerated on its western flank and reduced to the east of the hill. The shear across the hill was of the order of 3 to 5 cm s^{-1} . Spatial inhomogeneities in the far-field flow and its temporal variability made quantifying the topographic component in the flow disturbance difficult and the failure of the current meters at other deep levels precluded a measurement of the vertical attenuation in the topographic velocity field. Despite these problems a topographically generated perturbation was measured and its horizontal structure and energetics determined.

CTD profiles from sites around and over the hill showed a doming of isotherms over the topography with potential temperature at the top of the hill about equal to those at the abyssal plain 500 m below. The single station showing the cold water over the hill was separated by only 5 km from a station on the abyssal plain showing no detectable topographic influence. The implied geostrophic shear between the two stations was $\sim 2 \text{ cm s}^{-1}$, comparable to the measured shears in the far field. The distinction between the station on top of the hill and the mean of all the far-field stations decreased with increasing height above the bump summit level and at 4200 dbar (800 m above the hill top) was entirely masked by other large-scale disturbances in the density field.

A difficulty in modelling processes near the sea bed occurs because of the weak and variable stratification in the deep water and the presence of near-bottom homogeneous layers. Using a slowly varying N as a function of depth produces vertical profiles of pressure, density, and relative vorticity perturbations that resemble closely the observed profiles of these variables both in magnitude and in the nature of their vertical decay.

The practical difficulties in performing an experiment such as was attempted here are great. Variations of all the physical quantities are small and with even the best calibration procedures the variations are close to the limit of resolution of present instrumentation.

The choice of a small isolated hill represents only a first step towards the study of topographic influences around more generalized rough topography but the experiment has shown that even in isolation it can be difficult to separate the truly topographically induced signals from those impressed externally by inherent mesoscale variability of the ocean.

Neutrally buoyant floats have proved invaluable in the mapping of the near-bottom flow field, though there are uncertainties in ballasting, and as a result of vertical water movement over the hill, the floats' property of remaining on a constant pressure surface imply that the trajectories may not be truly Lagrangian. Floats capable of telemetering their height above the sea bed will be a useful tool in the future study of benthic processes.

The study has revealed that vertical profiles of density need to be made close to the topography with a horizontal separation of the order of 1 km or less to resolve the horizontal structure. This is a hazardous procedure and the best approach is likely to be achieved by slowly towing a CTD profiler and repeatedly lowering and raising the instrument through the lowest 1000 m or so of the water column.

The fact that a small hill such as that studied here has a detectable influence up to about three times its height above the neighbouring abyssal plain and to a horizontal distance about three times its width suggests that features such as this and those of greater size may have a profound influence on mixing processes in the deep ocean.

Acknowledgements—We wish to acknowledge the invaluable assistance of our colleagues at I.O.S. The authors are grateful to Dr J. C. SWALLOW, Principal Scientist on *Discovery* Cruise 70, and Dr D. J. WEBB, who played essential roles in the planning and execution of the experiment. Without their hard work in the early stages, the writing of this paper would not have been feasible. The expertise of Messrs J. CHERRIMAN, N. W. MILLARD and J. MOOREY ensured the high quality of the observations. The work would not have been possible but for the help of the officers and crew of the R.R.S. *Discovery*. One of the authors (R.H.) thanks the Natural Environment Research Council for a Fellowship that made possible a stimulating year at I.O.S. and acknowledges the further support supplied by the Atlantic Oceanographic Laboratory in order to finish the study. The work of another author (H.E.H.) is supported by the Ministry of Defence (Procurement Division).

REFERENCES

- BELL T. H. (1975) Statistical features of sea-floor topography. *Deep-Sea Research*, **22**, 883–892.
- BELL T. H. (1979) Mesoscale sea floor roughness. *Deep-Sea Research*, **26**, 65–76.
- BROWN N. L. and G. K. MORRISON (1978) WHOI/Brown conductivity, temperature and depth microprofiler. Woods Hole Oceanographic Institution, Technical Report 78–23. (Unpublished document.)
- DEFANT A. (1961) Currents in a strait. *Physical oceanography*, **1**, 513–543. Pergamon Press.
- HENDRY R. M. and A. J. HARTLING (1979) A pressure-induced direction error in nickel-coated Aanderaa current meters. *Deep-Sea Research*, **26**, 327–335.
- HIDE R. (1961) Origin of Jupiter's great red spot. *Nature*, **190**, 895–896.
- HOGG N. G. (1973a) On the stratified Taylor column. *Journal of Fluid Mechanics*, **58**, 517–537.
- HOGG N. G. (1973b) The preconditioning phase of MEDOC 1969-II. Topographic effects. *Deep-Sea Research*, **20**, 449–459.
- HOGG N. G., E. J. KATZ and T. B. SANFORD (1978) Eddies, islands and mixing. *Journal of Geophysical Research*, **83**, C6, 2921–2938.
- HUPPERT H. E. (1975) Some remarks on the initiation of inertial Taylor columns. *Journal of Fluid Mechanics*, **67**, 397–412.
- HUPPERT H. E. and K. BRYAN (1976) Topographically generated eddies. *Deep-Sea Research*, **23**, 655–679.
- HUPPERT H. E. and M. E. STERN (1974) The effect of side walls on homogeneous rotating flow over two-dimensional obstacles. *Journal of Fluid Mechanics*, **62**, 417–436.
- MEINCKE J. (1971) Observation of an anticyclonic vortex trapped above a seamount. *Journal of Geophysical Research*, **76**, 7432–7440.
- MENARD H. W. (1964) *Marine geology of the Pacific*, McGraw-Hill, 271 pp.
- MORSE P. N. and H. FESHBACH (1953) *Methods of theoretical physics*, McGraw-Hill, 1978 pp.
- ROBERTS D. G., N. G. HOGG, D. G. BISHOP and C. G. FLEWELLEN (1974) Sediment distribution around moated seamounts in the Rockall Trough. *Deep-Sea Research*, **21**, 175–184.

- RONA P. A., R. N. HARBISON and S. A. BUSH (1974) Abyssal hills of the eastern central North Atlantic. *Marine Geology*, **16**, 275-292.
- SWALLOW J. C. (1973) The second MODE leg of R.R.S. *Discovery*. *Mode Hot Line News*, **33**, 1-2.
- SWALLOW J. C. (1977) An attempt to test the geostrophic balance using Minimode current measurements. *A voyage of discovery*, George Deacon 70th Anniversary Volume, M. ANGEL, editor. *Deep-Sea Research* (supplement), pp. 165-176.
- SWALLOW J. C. and B. V. HAMON (1960) Some measurements of deep currents in the eastern North Atlantic. *Deep-Sea Research*, **6**, 155-168.
- SWALLOW J. C., B. S. McCARTNEY and N. W. MILLARD (1974) The Minimode float tracking system. *Deep-Sea Research*, **21**, 573-595.
- VASTANO A. C. and B. A. WARREN (1976) Perturbations to the Gulf Stream by *Atlantis II* seamount. *Deep-Sea Research*, **23**, 681-694.
- WORTHINGTON L. V. and W. G. METCALF (1961) The relationship between potential temperature and salinity in deep Atlantic water. *Rapport et procès-verbaux des réunions. Conseil permanent international pour l'exploration de la mer*, **149**, 122-128.